Momentum Search Algorithm for Analysis of Fuel Cell Vehicle-to-Grid System with Large-scale Buildings

Padhmanabhaiyappan Sivalingam and Madhusudanan Gurusamy

***Abstract*—The design and analysis of a fuel cell vehicle-to-grid (FCV2G) system with a high voltage conversion interface is proposed. The system aims to maximize the utilization of fuel cell vehicles (FCVs) as distributed energy resources, allowing them to actively participate in the energy market. The proposed FCV2G system has FCVs, power electronics interfaces, and the electrical grid. The power electronics interfaces are responsible for converting the low-voltage output of the fuel cell stack into high-voltage DC power, and ensuring efficient power transfer between the FCVs and the grid. To optimize the operation of the FCV2G system, the momentum search algorithm (MSA) is employed. By applying MSA, the FCV2G system can achieve optimal power dispatch, considering factors such as energy efficiency, grid stability, and economic feasibility. The proposed method is tested in MATLAB. The best MSA and dynamic load profile solutions are run for 24 h and the results show that 100% import of FCVs 51.0% more than 100% electric vehicle. Peak-cutting and vehicle-to-grid service revenue are 30.5% and 95.0% greater, respectively. Low discharge loss, high capacity, and high discharge power are the main advantages of FCVs. The benchmark FCVs ratio of 15% is used for sensitivity analysis. The findings reveal that the overall advantages of FCV2G are improved.**

***Index Terms*—Continuous conduction mode, DC-DC converter, discontinuous conduction mode, fuel cell vehicle, utility-grids, vehicle-to-grid**.

I. Introduction

A. Research Motivation

Electric vehicles (EVs) are expanding quickly, which gives elective answers for homegrown, modern applications and energy demand [1].

Received: April 10, 2023
Accepted: October 3, 2023
Published Online: March 1, 2024
Padhmanabhaiyappan Sivalingam (corresponding author) is with the Department of Electrical & Electronics Engineering, SRM Valliammai Engineering College, Potheri, Tamil Nadu 60320, India (e-mail: padmanbha0719@gmail.com).
DOI: 10.23919/PCMP.2023.000274

The way the vehicles spends a considerable time of the day in the recreation area supports better utilization of these frameworks in this time period [2]. The prospective study of fuel cell vehicle-to-grid (FCV2G) system with large buildings is crucial and challenging [3]. Hydrogen fuel cells in the FCV2G system can decrease greenhouse gas emissions and air pollution [4], [5]. By studying its potential in big buildings [6], it may help prevent climate change and create sustainable energy solutions [7], [8]. The implementation of FCV2G systems can have significant economic benefits [9]. By analyzing its potential in large-scale buildings, it can provide valuable insights into the financial viability and feasibility of the system, potentially attracting investments and creating new business opportunities [10]. FCV2G system can enhance the resilience of the energy grid by providing a decentralized and flexible energy storage solution [11], and it can contribute to ensuring a more reliable and resilient energy supply in the face of disruptions or emergencies [12]. The analysis of FCV2G systems in large-scale buildings requires a deep understanding of various cutting-edge technologies, including fuel cells, energy storage, and smart grid management.

B. Literature Review

Several research works presented in literatures are based on proportional-integral derivative (PID) controller for non-linear control system using various methods and features.

Reference [13] presents a well-to-wheel and net cost of ownership approach and compares the CO_2 emission, energy consumption, and cost of fuel cell vehicles (FCVs) with alternative power trains and its practices, depicting the scale of cost gaps. The presented method enhances the limitations of expected future growth of hydrogen EVs and fuel cell EVs based on lower cost and carbon emission. Fuel cell (FC) life cycle assessment (LCA) should concentrate on hydrogen storage tank and carbon fiber manufacture [14]. Reference [15] introduces a time-varying FCVs hydrogen refueling demand for medium, light, heavy duty vehicles by utilizing the electrolysis systems transmitted during west-

ern U.S. power system. Reference [16] presents the economic potential of FC V2G system for promoting FCVs to high level. Reference [17] presents a boost for promoting FCVs by examining the economic possibility of the FCV2G system. First, a major Japanese large scale building is chosen as the study target while vehicle agent gives power grid service. Next, Monte Carlo simulation shows vehicle condition and visit time differences with the discharging approach established. Reference [18] introduces an increasing characteristic of FCVs through providing vehicle-to-grid (V2G) technologies and the combination of electricity and transportation networks. The FC virtual to grid system with the introduced converter is examined for various modes of operation for evaluating smooth transfer of energy with maximal power enhancing capability. In [19] an online energy management system (EMS) related to increased power frequency method is presented to meet the requirement of loads and to improve the effectiveness of functioning FCVs.

C. Necessity of the Research Based on Challenges of the Literature

The research on the potential analysis of FCV2G system with large-scale buildings is necessary due to the challenges faced. Understanding and addressing these challenges are crucial to the successful implementation of such a system. One of the main challenges is the lack of available knowledge specifically focusing on the FCV2G system with large-scale buildings. While there are ample researches on FCVs, grid integration, and building energy management systems, there are limited studies that explore the integration of these elements in a large-scale setting. This research gap needs to be filled in order to give useful feasibility insights, benefits, and challenges of implementing FCV2G system in the context of large-scale buildings. Another challenge is the complexity of the FCV2G system itself. The system involves multiple components, including FCVs, electric grid, and large-scale buildings, each with their own unique characteristics and requirements. Analyzing the potential of such a system requires a thorough understanding of the technical, economic, and environmental aspects of all these components, as well as their integration. Furthermore, the analysis needs to consider the dynamic nature of the system, accounting for factors like vehicle availability, building energy demand, and grid requirements. Additionally, the existing researches lack comprehensive studies that evaluate the potential benefits and challenges specific to large-scale buildings, which have distinct energy consumption patterns, electrical infrastructure, and operational constraints compared to smaller buildings. Therefore, it is essential to conduct researches that specifically address these factors to give insights on the possible advantages and obstacles of integrating FCV2G technology in large-scale structures.

D. Novelty and Main Contributions of the Paper

The novelty and contribution of this work lie in the design and analyses of FCV2G system with a high voltage conversion (HCV) in particular.

1) The proposed method transforms low-voltage FC stack output into high-voltage DC power through a high voltage conversion interface. This allows for easy integration of FCVs into the electrical grid and maximizes their utilization as distributed energy resources

2) The system also incorporates a power electronics interface that ensures efficient power transfer between the grid, and the FCVs.

3) By enabling FCVs to actively participate in the energy market, the proposed FCV2G system maximizes the use of FCVs as distributed energy resources.

4) The incorporation of the momentum search algorithm (MSA) allows for the optimal power dispatch of the FCV2G system.

E. Organization and Structure of the Paper

Section I shows the introduction. Sections II explains the overview of FCV2G, while Section III describes the proposed approach. Section IV demonstrates the results and discussions. Finally, Section V concludes the paper.

II. OVERVIEW OF FCV2G

In recent years, the V2G system has been developed which benefits the electric grid, e.g., improvement in quality, saving energy and flexible operation. Due to the large energy storage capacity potential, EVs are considered as distributed resources. The architecture of FCVs is shown in Fig. 1. As seen, the FCVs and V2G are two main parts in this system, while the FCVs is attached to grid by using V2G. The fuel cell is defined as energy supplier that provides energy during driving time and to grid during parking time through V2G [20].

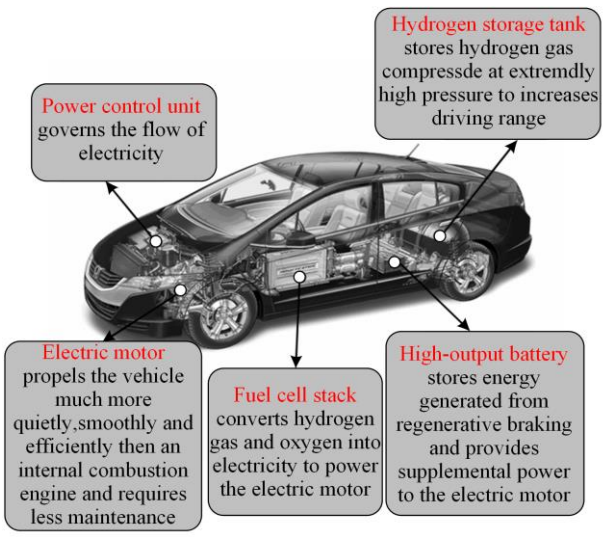

Fig.1. Architecture of fuel cell EVs.

The V2G unit contains a DC-DC converter and a DC to AC inverter. The DC to AC inverter transfers DC power into AC based on the requirement of the grid, whereas the DC to DC converter regulates the DC-link voltage while also satisfies maximum generation of FC power. Figure 2 depicts the structure of a typical FCV2G system.

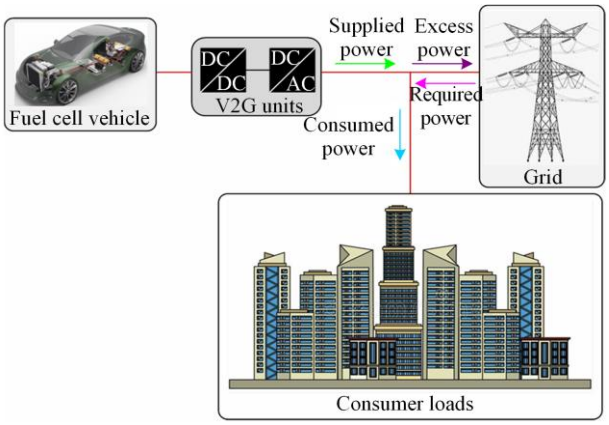

Fig. 2. Structure of a typical FCV2G system.

In a single-phase grid system, only a minimal number of inverter structures are used during the DC to AC conversion process for V2G technology. Also, this structure can use three-level three-phase inverter, single-stage inverter, conventional full-bridge inverter and asymmetrical three-level inverter etc. The full-bridge inverter architecture was chosen because it is low-cost and has a straightforward control technique. Circuit diagram of fuel cell V2G with high-voltage conversion interfaces is shown in Fig. 3. For maximum power tracking of voltage regulation and energy transfer, the DC-DC converter plays an important role in V2G unit. The topologies can be unidirectional, bidirectional, isolated and non-isolated types. The bidirectional DC-DC converter permits the power to flow on both energy sources to the grid, which is frequently utilized in the batteries in EV or plug-in hybrid electric vehicle (HEV). The unidirectional converter is usually preferred because the energy flows from pure FC to grid while compared with bidirectional converter.

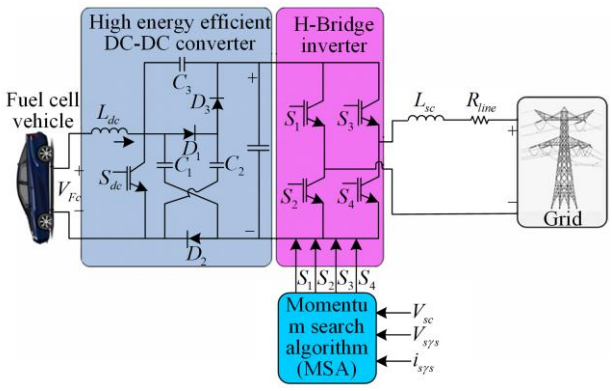

Fig. 3. Circuit diagram of FCV2G with high-voltage conversion interfaces.

In fuel cells, many unidirectional DC-DC converters are used. Some of the boost converters used include interleaved boost converters [21], conventional boost converters, dual-switch boost converters, multi-phase interleaved boost converters, isolated active-passive full-bridge converters, switched capacitor based on H-type boost converters, etc. Within these topologies, the conventional boost converter contains a higher ripple voltage and a lower voltage conversion ratio. A 3-leg boost converter is utilized to reduce voltage ripple, while a 4-leg floating interleaved boost converter is used for efficient reductions. Multi-phase interleaved converters with low voltage conversion ratios reduce output voltage ripple. For FC with low output voltage, high voltage conversion ratio is essential. By controlling transformer turn ratio, the isolated active-passive full-bridge converter increases voltage ratio transmission. However, when a transformer is introduced, the performance of the system is decreased. The switched capacitor outperforms the transformer with simpler structure to attain high-voltage gain. The switched-capacitor model is used to design and create high-gain DC to DC converters for various topologies. Based on dual-switched capacitor, the proposed DC to DC converter has poor regulation for output voltage. Recently, to enhance the conversion ratio, the capacitor clamped H-type converter is proposed but it needs additional electronic component. A new DC to DC converter topology is proposed to reduce the count of electronic switches, and is further elaborated in the following sections.

A. Basic Operation of Proposed Converter for FC Vehicle-to-grid

As a distributed energy generating system to load/grid, the FCV2G's high-gain and high-efficiency hybrid-switched capacitor converter is used. Power flow from proton exchange membrane FC (PEMFC) to load or grid gives high-voltage conversion ratio for proposed converter compared to traditional boost converter. In similar systems, improving the voltage gain of the DC to DC converter is critical when using FC as energy sources with low output voltage.

1) States of Equivalent Circuit and Switching

According to the inductor current, the proposed converter contains 2 distinct conduction modes. The converter functions in continuous conduction mode (CCM) when the inductor current flows continuously, whereas it works in discontinuous conduction mode (DCM) when the inductor current reaches zero for part of the switching period. The proposed converter operates in DCM because it is more convenient to switch among activity modes [22].

The state of switching and current flows are shown in Fig. 4. In CCM, Figs. 4 (a) and (b) display the current flow path for ON-state and OFF-state, respectively. Fig. 4(c)

depicts OFF-state in DCM. While the system functions in DCM, it has the ability to operate in CCM mode.

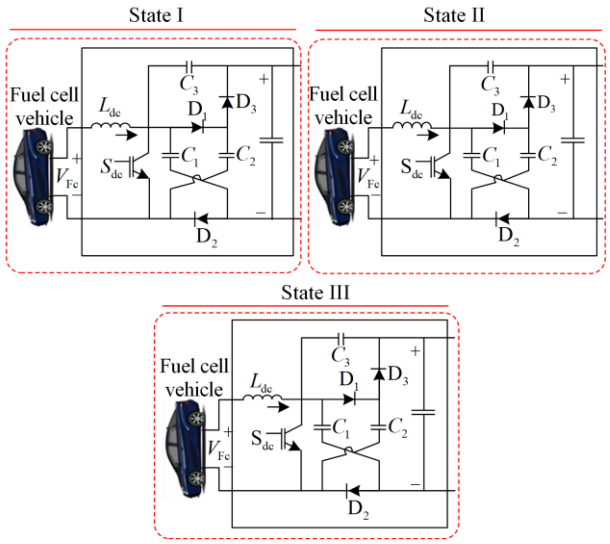

Fig. 4. Current flow path in continuous conduction mode for three different cases. (a) ON-state. (b) OFF-state. (c) OFF-state in discontinuous conduction mode.

Figure 5 depicts the operational stage of proposed converter. During switching cycle for CCM, the converter has two functional phases. Here, D is denoted as duty cycle, and the direct current links with the converters output voltage are defined. The value differs between 0 and 1 based on selected output voltage.

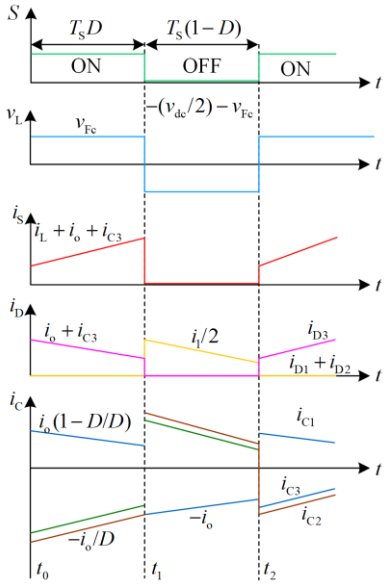

Fig. 5. Operational stage of proposed converter.

2) Operation Principles

Stage 1: $[T_0 - T_1]$

In T_0, switch S is turn ON and at the same time D_3 is said to be forward-biased. Due to negative voltage through C_3 capacitor, D_1 and D_2 are turned off. C_2 and C_3 are connected in parallel and have similar voltage as C_1 during the time interval. C_1 and C_2 supply the load, while C_2 charges C_3 [23]. The relationship between the output voltage and the voltages across the capacitors are described as:

$$v_{c_1} = v_{c_2} = v_{c_3} = v_c \tag{1}$$

$$v_{Fc} = (1-D)\, v_c \tag{2}$$

$$v_{dc} = v_{c2} + v_{c3} = 2v_c \tag{3}$$

where the voltages of capacitor C_1, C_2 and C_3 are represented as v_{c_1}, v_{c_2} and v_{c_3}; v_c is the converter voltage; v_{dc} and v_{Fc} implies the output voltages of the proposed converter and fuel cell [24].

Stage 2: $[T_1 - T_2]$

In T_1, S is off, so does D_3 due to negative voltage through C_3. While D_1 and D_2 are said to be ON, the inductor energy is supplied to the load via the current path. During the interval of time, C_2 and C_3 are linked in parallel, and C_1, C_2 have similar voltage but are polarized negatively, while C_3 has same voltage amplitude. Their relationship to the DC-link voltage is shown as follows:

$$v_{dc} = v_{c_1} - v_{c_3} = v_{c_1} - v_{c_3} \tag{4}$$

At CCM, the proposed converter's gain is stated as:

$$Gain = \frac{v_{dc}}{v_{Fc}} = \frac{2}{(1-D)} \tag{5}$$

To improve maximal power from FC, the perturb and observe approach is used for controlling the duty-cycle of the DC to DC converter. The voltage and power characteristic of FC depends on related techniques. The controller observes voltage and current to execute quick power production of the FC. By using the operating conditions, the output voltage of the FC and the perturb controller is given a direction, and the power provided by the FC is monitored. If the power is positive, the controller continually disrupts the FC's output voltage in the same direction. The operation voltage perturbs are achieved through the duty cycle, which is expressed as:

$$D_{New} = D_{Old} + \Delta D, \quad P > P_{Old} \tag{6}$$

$$D_{New} = D_{Old} - \Delta D, \quad P > P_{Old} \tag{7}$$

$$D_{New} = D_{Old}, \quad P = P_{Old} \tag{8}$$

$$d_2 = \frac{D v_{Fc}}{v_c - v_{Fc}} \tag{9}$$

where D_{New} is new duty cycle; D_{Old} is old duty cycle; v_{Fc} is fuel cell voltage voltage; P_{Old} is the old power value in MPPT method; and d_2 is the value of diodes in the DC-DC converter.

The average inductor current i_{Fc} is:

$$i_{\mathrm{Fc}} = \frac{v_{\mathrm{Fc}} D^2 t_{\mathrm{s}}}{2l}\left[\frac{v_{\mathrm{dc}}/v_{\mathrm{Fc}}}{v_{\mathrm{dc}}/v_{\mathrm{Fc}} - 2}\right] \tag{10}$$

The gain in DCM is computed as

$$Gain_{\mathrm{dcm}} = 1 + \sqrt{1 + \frac{D^2}{k}} \tag{11}$$

where the dimensionless parameter k is defined as:

$$k = \frac{2l}{r_{\mathrm{Load}}\, t_{\mathrm{s}}} \tag{12}$$

where r_{Load} is the equivalent load value in the converter; t_{s} is the temperature; l is the value of inductor.

Then the boundaries between the CCM and DCM can be computed:

$$i_{\mathrm{Fc}} < \Delta i_l \tag{13}$$

where Δi_l is the current ripple of inductor in DC-DC converter and it can be computed as:

$$\Delta i_l = \frac{i_{l(\mathrm{Peak})}}{2} = \frac{v_{\mathrm{Fc}} D t_{\mathrm{s}}}{2l} \tag{14}$$

where $i_{l(\mathrm{Peak})}$ is the peak current of inductor in DC-DC converter.

The boundary condition is attained as

$$k < k_{\mathrm{Cr}} = \frac{V_{\mathrm{dc}}/V_{\mathrm{Fc}} - 2}{(V_{\mathrm{dc}}/V_{\mathrm{Fc}})^3} \tag{15}$$

where the critical dimensionless parameter is denoted as k_{Cr}. The converter operation mode is determined as

$$\begin{cases} k < k_{\mathrm{Cr}}, & \text{Operates in DCM} \\ k > k_{\mathrm{Cr}}, & \text{Operates in CCM} \end{cases} \tag{16}$$

B. Design of FCV2G

Here, the FCV2G system and its design are elaborated. The system contains V2G unit, FCVs, electric grid and dynamic load. During parking, the FCVs distribute the energy to electric grid and dynamic load [25].

1) Fuel Cell Stack

The FC unit converts chemical energy to electricity using hydrogen fuel [26]. The fuel cell has many types, but in recent days PEMFC is chosen due to the operational range in temperature and high power advantages. The PEMFC contains 3 main units: anode, cathode, and electrolyte. This electrolyte is produced by the polymer electrolyte membrane. The following steps show the performance of FC stack.

Step 1: In anode side, the positive ion charge and negative electron are generated from hydrogen through a catalyst.

Step 2: Current production involves proton charge towards the electrolyte and electron charge above the circuit.

Step 3: Positive ions and electrons react with oxygen, water gas, and heat. At this point, the maximal voltage produced through the PEMFC is nearly 0.7 V. By connecting cells in series, the required voltage for the applications is achieved.

PEMFC equivalent circuit is depicted in Fig. 6. And the generated cell voltage is derived as:

$$v_{\mathrm{Fc}} = v_{\mathrm{Nerst}} - (v_{\mathrm{Com}} + v_{\mathrm{act}} + v_{\mathrm{Ohmic}}) \tag{17}$$

where voltages of concentration, ohmic losses and activation are represent as v_{Com}, v_{Ohmic}, and v_{act}, respectively; v_{Nerst} specifies the reversible (Nernst) output voltage potential. v_{Com}, v_{act}, and v_{Ohmic} are given as:

$$v_{\mathrm{Com}} = -B\ln\left[1 - \frac{i_{\mathrm{Fc}}}{i_{\mathrm{Max}}}\right] \tag{18}$$

where B is denoted as Tafel coefficient.

$$v_{\mathrm{act}} = \xi_1 + \xi_2 t_{\mathrm{Fc}} + \xi_2 t_{\mathrm{Fc}} \ln\left(\frac{P_{\mathrm{O_2}}}{5.08\times10^6 \times \mathrm{e}^{-(498/t_{\mathrm{Fc}})}}\right) + \xi_4 t_{\mathrm{Fc}} \ln(i_{\mathrm{Fc}}) \tag{19}$$

$$v_{\mathrm{Ohmic}} = (r_{\mathrm{m}} + r_{\mathrm{c}})\, i_{\mathrm{Fc}} \tag{20}$$

where t_{Fc} denotes the FC temperature; $P_{\mathrm{O_2}}$ denotes the partial pressures of oxygen; i_{Max} and i_{Fc} are the maximum current and cell current of PEMFC, respectively; while r_{c} and r_{m} denote the contact and membrane resistances; ξ_1 ξ_2 and ξ_4 are the empirical coefficients of every cell, respectively.

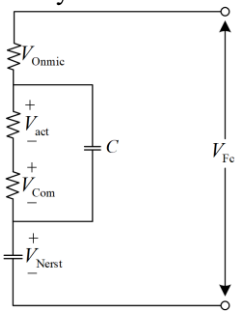

Fig. 6. PEMFC equivalent circuit.

2) V2G Interface

The DC output voltage of FC is varied based on pressure, temperature, etc. In V2G interface system, the DC-DC converter and inverter of DC to AC are utilized. The DC to DC converter keeps the DC voltage in the indicated level with maximum power point tracking generation from the stack of fuel cell. The DC-AC inverter is utilized for transferring DC to AC side.

To send FC power to dynamic loads and the grid, a single-phase H-bridge inverter is employed. This inverter has four electronic switches using either IGBT or MOSFET. The operation is controlled by switching the inverter to fulfill the power transfer. The hysteresis modulation approach is used, with the switching process as follows:

$$\begin{aligned} i_{\mathrm{Err}} > +H \quad &\Rightarrow \begin{cases} s_1, s_4 = 1 \\ s_2, s_3 = 0 \end{cases} \\ i_{\mathrm{Err}} > +H \quad &\Rightarrow \begin{cases} s_1, s_4 = 0 \\ s_2, s_3 = 1 \end{cases} \end{aligned} \tag{21}$$

where the hysteresis band is H and the error current signal i_{Err} is attained as follows:

$$i_{\mathrm{Err}} = i_{\mathrm{Err,D}}\cos(\omega t) - i_{\mathrm{Err,Q}}\sin(\omega t) \tag{22}$$

where the error signals of current in d-q frame are $i_{\mathrm{Err,Q}}$ and $i_{\mathrm{Err,D}}$. This error signals in d-q frame are derived as:

$$i_{\mathrm{Err,D}} = i_{\mathrm{Ref,D}} - i_{\mathrm{Sys,D}} \tag{23}$$

$$i_{\mathrm{Err,Q}} = i_{\mathrm{Ref,Q}} - i_{\mathrm{Sys,Q}} \tag{24}$$

where $i_{\mathrm{Ref,D}}$ and $i_{\mathrm{Ref,Q}}$ imply current error signals in the d-q frame, which are also known as active and reactive current errors.

The component of active current is gained through controlling active power fed into grid. The control of active power is recognized by the proportional-integral (PI) controller. In d-q frame, $i_{\mathrm{Sys,Q}}$ and $i_{\mathrm{Sys,D}}$ are injected using the current signals also referring to as active current and reactive current. This inserted current is calculated and converted in to d-q and α-β frames.

3) Load Profile

The load profile employed in the suggested technique is detailed here. Based on the day to day local power consumption, the data are constructed and designed by dynamic load profile [27]. The electronic and electrical loads, such as air conditioner, lightning, computers and heater etc., are taken as the description for the design of load.

C. Forecasting Methodologies

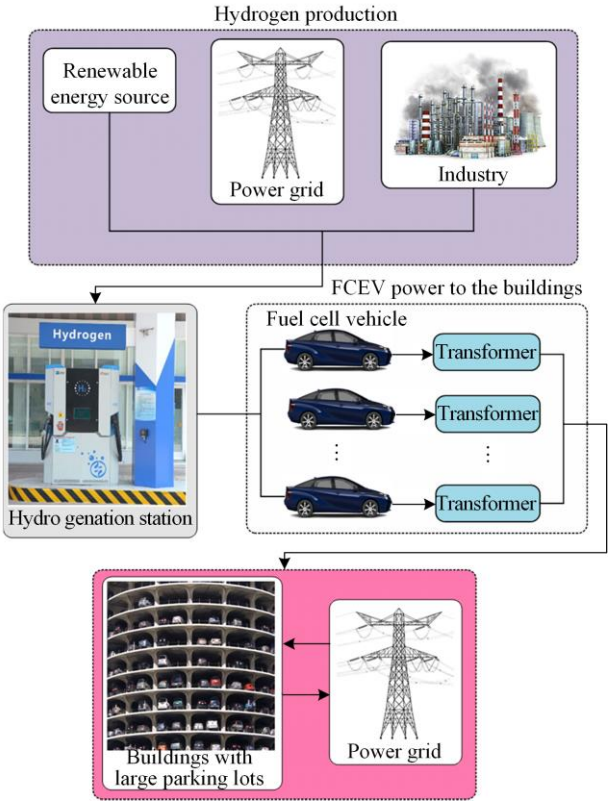

Fig. 7. Concept of FCV2G.

The production of hydrogen systems are classified by using primary energy types, like electrochemical, biological, electrical, photochemical, photonic, electro thermal, thermo chemical and thermal, which are some of the most commonly used sources of hydrogen [16]. The concept of FCV2G is shown in Fig. 7. Compared to many researches, the hydrogen production is efficient, particularly hydrogen production with electricity/renewable energy [28].

1) Related Technologies of FC Vehicle

The exploration of fuel cells consolidates with electric vehicles and has its own use and application modes. FCVs have drawn increased considerations due to less emission, quick refueling and calm driving [29]. Notwithstanding the advancement, quantity of hydrogenation stations are excessively limited and cost are high. Consequently, the exploration of FCVs primarily serves as the centers of these perspectives.

2) Application of FCV2G

FCVs structure an energy aggregator but the structures with huge parking areas can partake in V2G administrations with grid. As of now, the examination on FCV2G is somewhat limited, however there contains lots of V2G and vehicle to home researches with PEVs and HEVs, which have incredible reference esteem [30].

3) Carbon Emission Pricing

As power produced by FCVs from FC reactors contains no CO_2 emission, when considering FCV2G, the effects of CO_2 emission price in general income ought to be considered. As a significant proportion of global energy saving and lessening the carbon emission, the price of carbon emission is the exploration area of interest in these days. Fossil fuel byproducts are presently normally utilized for near innovation or building life cycle examination [31].

4) Charge and Discharge Model

$$SOC_{T+1}^{I} = SOC_{T}^{I} + (p_{CH}^{I} \times ICH_{T}^{I} - p_{\mathrm{Dis}}^{I} \times IDIS_{T}^{I}) \tag{25}$$

where discharging signal is denoted as $IDIS_T^I$, charging signal is ICH_T^I; discharging and charging capacities are p_{Dis}^I and p_{CH}^I, respectively. Capacity to participate is denoted as CP_T and total amount of charging and discharging is denoted as ECH_T and $EDIS_T$, given as:

$$ECH_T = \sum_{I=1}^{N} (ICH_T^I \times p_{\mathrm{CH}}^I) \tag{26}$$

$$EDIS_T = \sum_{I=1}^{N} (IDIS_T^I \times p_{DIS}^I) \tag{27}$$

$$CP_T = \sum_{I=1}^{N} (SOC_T^I - Limit_{CP}) \tag{28}$$

where $Limit_{\mathrm{CP}}$ specifies the maximal discharging capacity limit.

5) Establishing Economic Income Model

The structure with big parking garage is viewed as an example, from one perspective, to give reasonable discharge costs to vehicles, and then to give V2G administrations to the grid [17]. For this situation, the increase in its structure $Income_{\text{Total}}$ is expressed as:

$$Income_{\text{Total}} = Income_{\text{Pr}} + Income_{\text{V2G}} - Spend_{\text{S}} - Spend_{\text{e}} \tag{29}$$

where V2G service income is signified as $Income_{\text{V2G}}$; income by reducing peak demand of electricity is denoted as $Income_{\text{Pr}}$; discharging of electricity price is denoted as $Spend_{\text{e}}$; and spending to pay is indicated as $Spend_{\text{S}}$. $Income_{\text{Pr}}$ is derived as:

$$Income_{\text{Pr}} = Price_{\text{Basic}} \times \Delta load_{\text{Peak}} \tag{30}$$

where the basic capacity of income and ancillary service income from the participation in V2G is denoted as $Price_{\text{Basic}}$; $\Delta load_{\text{Peak}}$ is the increment value of peak load. And $Spend_{\text{S}}$ is derived as:

$$Spend_{\text{S}} = (Price^{J}_{\text{Dis}} - Price^{J}_{\text{Co}_2} - Price_{\text{Normal}}) \times EDIS_{T} \tag{31}$$

where J represents the discharged vehicle for FCVs; price of reducing carbon emissions is signify as $Price^{J}_{\text{Co}_2}$; and discharge price is denoted as $Price^{J}_{\text{Dis}}$ by utilizing electricity produced from clean energy sources [18]. Price of building electricity is represented as $Price_{\text{Normal}}$ which is purchased from the power grid.

$$Price^{\text{EV}}_{\text{Dis}} = Price^{\text{EV}}_{\text{Add}} + \frac{Cost_{\text{Battle}}}{K \times number_{\text{Cycle}} \times SOC_{\text{Max}} \times dod} \tag{32}$$

where the cyclic multiple is denoted as K; the number of cycles is indicated as $number_{\text{Cycle}}$; an extra discharge price for electric vehicle is indicated as $Price^{\text{EV}}_{\text{Add}}$; the total cost of battery is signify as $Cost_{\text{Battle}}$; and the depth of discharge is represent as dod.

$$Price^{\text{EV}}_{\text{Add}} = Price^{\text{FCV}}_{\text{Add}} + \frac{Cost_{\text{FC}} \times e_{\text{CO}_{\text{FC}}}}{365 \times \delta_{\text{Fc}}} \tag{33}$$

where the conversion of coefficient among daily fuel consumption and its electricity is specified as δ_{Fc}, and the capital recovery coefficient of FC is represent as $e_{\text{CO}_{\text{FC}}}$, and the net cost of FC is denoted as $Cost_{\text{FC}}$.

$$Spend_{\text{e}} = \frac{Cost^{J}_{\text{Dis}} \times e^{J}_{\text{CoDis}}}{365} \tag{34}$$

where e^{J}_{CoDis} specifies the capital recovery coefficient of discharge, and $Cost^{J}_{\text{Dis}}$ specifies the cost of discharge.

III. Proposed Methodology

A. Momentum Search Algorithm

The optimization process is done in time-discrete and artificial by using motion laws and momentum. In this system, problem constraints are borders. The utilized system contains solution body set with its position. Here, the possible solution is denoted as N Body mass is proportional to fitness function that is related to its position.

Step 1: initialization

Initialize the input parameters, like voltage and current.

Step 2: random generation

After initiation, the values are randomly created.

Step 3: fitness function

The fitness function depends on the objective function described by,

$$F_c = \text{Min}(P) \tag{35}$$

Step 4: From the initial position, a set of body along various mass seeks diverse position in space to reach optimal position. The motionless bodies are denoted as M, which are predetermined by the initial position problem. $X^{(D)}_{\text{I}}(t)$ specifies the line of the position of the dth dimension, and $X_{\text{I}}(t)$ specifies the position of the ith body in t time and was derived in (35).

$$X_{\text{I}}(t) = (X^{(1)}_{(\text{I})}(t), \cdots, X^{(D)}_{(\text{I})}(t), \cdots, X^{(N)}_{(\text{I})}(t)) \tag{36}$$

$$X^{(J)}_{\text{Min}} \leqslant X^{(J)}_{(\text{I})}(t) \leqslant X^{(J)}_{\text{Max}}, I = 1, \cdots, M;\ J = 1, \cdots, N \tag{37}$$

Step 5:

1) Updating the Mass of Solution Body

The $M_{\text{I}}(T)$ is used to measure the mass of bodies at the start of every iteration and depends on minimal fitness function of best value.

$$M_{\text{I}}(T) = \frac{Fit_{\text{I}}(T) - Worst(T)}{Best(T) - Worst(T)} \tag{38}$$

Here the objective function for $X_{\text{I}}(T)$ is $Fit_{\text{I}}(T)$. By utilizing (38), the mass is assigned to bodies along increasing appropriateness for reaching the optimal point. Thus, the values of $Worst(T)$ and $Best(T)$ are derived as:

$$Best(T) = \min_{J=1,\cdots,M} Fit_{I}(T) \tag{39}$$

$$Worst(T) = \min_{J=1,\cdots,M} Fit_{I}(T) \tag{40}$$

The mass is allotted for the bodies with improved fitness function. Each body returns to its control based on external body alteration. The best solution can move easier than the worst solution.

2) Mass and Speed of External Body

The mass of the external body in each iteration t is $M(T)$, and it is measured by:

$$M(T) = 1 - \frac{T-1}{t-1} \tag{41}$$

where the maximum count of iterations is denoted as t.

By using (41), the external body mass is one and in the last iteration, the constant rate is decreased until it reaches to zero. External body of the dth speed com-

ponent matches the *i*th system body in iteration t and is computed as:

$$u_{\mathrm{I}}^{(D)}(T)=R_{1}\left(1-\frac{T-1}{t-1}\right)u_{\mathrm{Max}}\times Sign(X_{\mathrm{Best}}^{(D)}(T)-X_{\mathrm{I}}^{(D)}(T)) \tag{42}$$

where u_{Max} specifies that the maximum external body speed is the limits in control variables. The random number with uniform distribution in [0, 1] is denoted as R_1 and is shown in (42). The presence of the random term is signified as $\left(1-\frac{T-1}{t-1}\right)u_{\mathrm{Max}}$ and external body speed is reduced at average time. $Sign\,(X_{\mathrm{Best}}^{(D)}(T)-X_{\mathrm{I}}^{(D)}(T))$ shows that for the best values the system body cannot move in opposite direction. $X_{\mathrm{Best}}^{(D)}(T)$ and $X_{\mathrm{I}}^{(D)}(T)$ specifies *d*th dimension of system body and greatest iteration fitness *t* and *i*th system body, $X_{\mathrm{Best}}^{(D)}-X_{\mathrm{I}}^{(D)}$, is the sign function that specifies bodies that cannot approach the finest of each iteration exactly while not moving in either directions. The external body momentum of *d*th component coinciding with the *i*th system body at *t* iteration is expressed as:

$$P_{\mathrm{I}}^{(D)}(T)=m(T)u_{I}^{(D)}(T) \tag{43}$$

3) Calculating the New Position of System Bodies after Collision

By using the kinetic and momentum energy conservation laws, after collision with the *i*th body in t time, the body speed is denoted as $(v_{\mathrm{I}}^{(D)}(T))$ and is calculated as:

$$m(T)u_{\mathrm{I}}^{(D)}(T)=M_{\mathrm{I}}(T)V_{\mathrm{I}}^{(D)}(T)+m(T)U_{\mathrm{I}}^{(D)}(T) \tag{44}$$

$$\frac{1}{2}m(T)(u_{\mathrm{I}}^{(D)}(T))^{2}=\frac{1}{2}M_{\mathrm{I}}(T)(V_{\mathrm{I}}^{(D)}(T))^{2}+\frac{1}{2}m(T)(U_{\mathrm{I}}^{(D)}(T))^{2} \tag{45}$$

$$v_{\mathrm{I}}^{(D)}(T)=\frac{2m(T)}{M_{\mathrm{I}}(T)+M(T)}u_{\mathrm{I}}^{(D)}(T) \tag{46}$$

where the body mass of the *i*th system and the *d*th dimension speed component are represented as $M_{\mathrm{I}}(T)$ and $v_{\mathrm{I}}^{(D)}(T)$; the external body mass before and after collision is $u_{\mathrm{I}}^{(D)}(T)$ and $u^{(D)}(T)$, respectively. Using the speed of system bodies after collision in (46) shows new position. The present position of each body is the addition of preceding positions, and thus, the percentage of speed after collision is denoted as:

$$X_{\mathrm{I}}^{(D)}(T+1)=X_{\mathrm{I}}^{(D)}(T)+R_{2}\,v_{\mathrm{I}}^{(D)}(T) \tag{47}$$

where the random number with a uniform distribution is specified as R_2 in [0, 1] range, and the speed of the *i*th body in the direction of the *d*th dimension in time T is $v_{\mathrm{I}}^{(D)}(T)$. Figure 8 shows the flowchart of the proposed method.

Step 6: Termination

The process continues until the optimal solution is achieved otherwise it goes to Step 3. Table I depicts the pseudo code for the MSA algorithm.

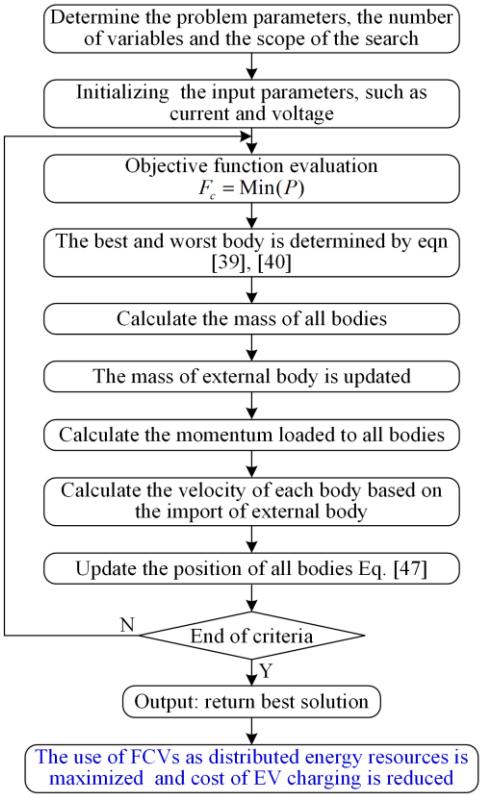

Fig. 8. Flowchart of the proposed approach.

TABLE I
PSEUDO CODE FOR THE MSA ALGORITHM

Start momentum search algorithm

Input: N, n, T, $X_{\min}$, and $X_{\max}$

Initialize the momentum search algorithm population $x_i(i=1,2,\cdots N)$

For iteration $=1:N$

Calculate the fitness function of each search agent.

Update *best* (*t*) and *worst* (*t*)

$Best\,(T)=\min_{I=1,\cdots,M} Fit_I(T)$ *and* $Worst(T)=\max Fit_I(T)$

Calculation of the mass of all bodies.

$$M_I(T)=\frac{Fit_I(T)-Worst(T)}{Best(T)-Worst(T)}$$

Update M

Calculate $u_I^{(D)}(T)$ for all bodies.

Calculate $P_I^{(D)}(T)$ for all bodies.

Update $v_I^{(D)}(T)$ for all bodies.

Update the position of each body.

Verify the new position with $X_{\min}$, and $X_{\max}$.

Save the best solution so far.

END iteration.

Output: return the best fitness value */

END momentum search algorithm

IV. Result and Discussion

Here, the simulation results of the proposed method and existing methods are studied. The momentum search algorithm for the potential analysis of FCV2G system with large scale buildings is analyzed. The proposed controller is run in MATLAB and its performance is examined.

Figure 9 depicts the clustering daily half-hour change curve centers. The clustering centers are organized from big to small, i.e., from L_1 to L_6. Based on the curves, the load changes are obtained.

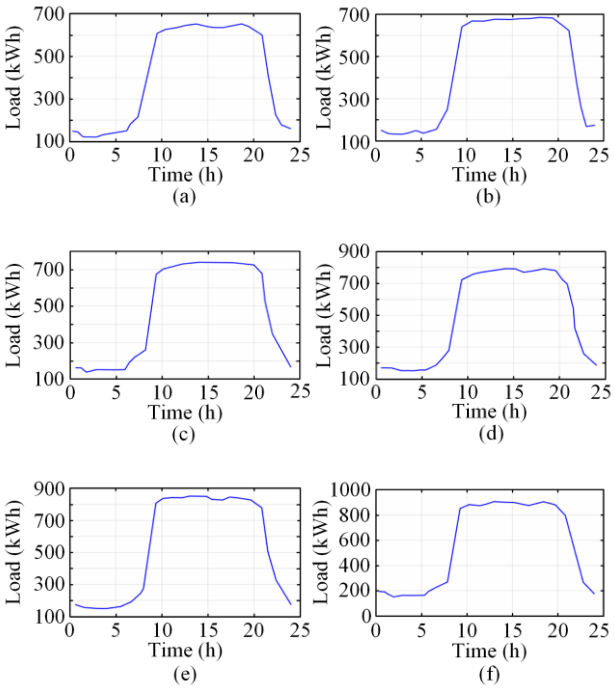

Fig. 9. Clustering daily half-hour change curve centers. (a) L_1. (b) L_2. (c) L_3. (d) L_4. (e) L_5. (f) L_6.

Figure 10 depicts the visit rate of vehicle in one week. In the following simulations, Monday marks another weekend as the changes are closer to the vehicles arriving from Monday to Saturday.

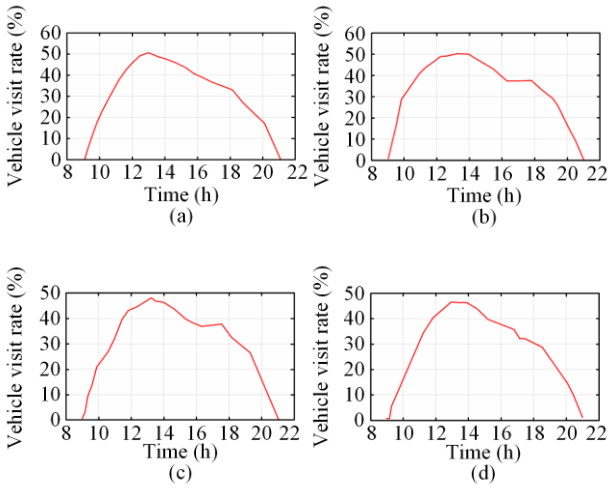

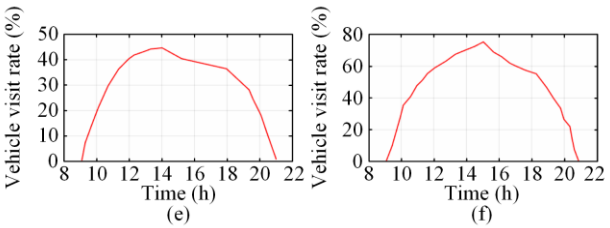

Fig. 10. Visit rate of vehicle in one week. (a) Sunday. (b) Monday. (c) Tuesday. (d) Wednesday. (e) Thursday. (f) Friday.

Figure 11 displays the driving distance probability density. When the probability is 0.406, the value of driving distance is 48 km. When the value of driving distance is 400 km, the probability approaches 0.

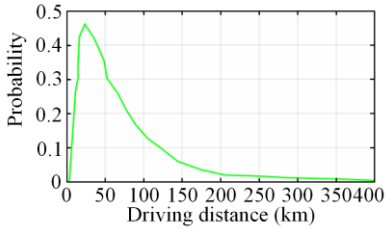

Fig. 11. Driving distance probability density.

Figure 12 depicts the residence time probability density curve. When time is 1.5 then the value of probability is 0.709, whereas when time is 2 the value of probability is 0.59, and it then gradually decreases to 0.

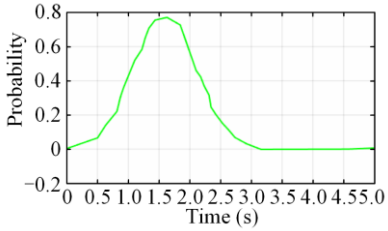

Fig. 12. Probability density curve of residence time.

Figure 13 depicts the investigation of loads with V2G for various FCVs. For 50 FCVs, the maximal visiting FCVs are accrued. When 400 fuel cell vehicles are installed, the discharge go beyond the power consumption of the building.

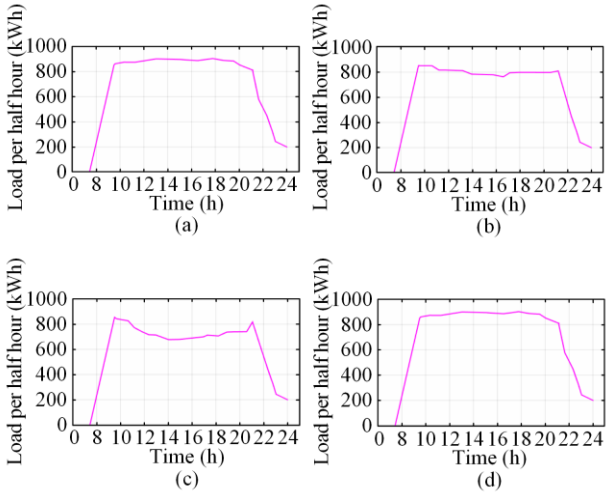

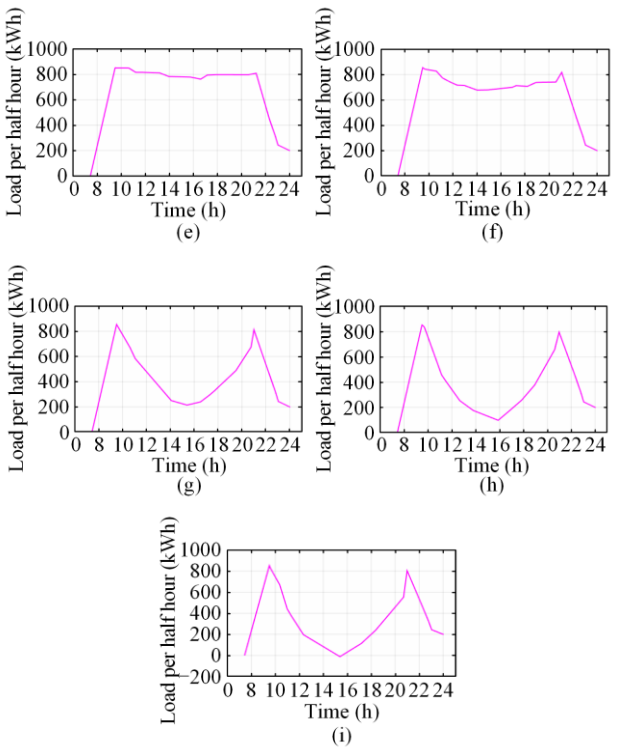

Fig. 13. Investigation of loads with V2G for various FCVs. (a) Basic load. (b) Load with V2G for 50 FCVs. (c) Load with V2G for 100 FCVs. (d) Load with V2G for 150 FCVs. (e) Load with V2G for 200 FCVs. (f) Load with V2G for 250 FCVs. (g) Load with V2G for 300 FCVs. (h) Load with V2G for 350 FCVs. (i) Load with V2G for 400 FCVs.

Figure 14 show the analyses of loads for different degrees of FCVs and EV. During fewer vehicles to grid discharge and peak-cutting effect, the EV charging demand is not known as peak valley gap. The percentage of FCVs and the discharge of V2G service are lowered. The final total income is less due to less total discharge cost. As a result, FCVs bring higher advantage than EV in V2G services.

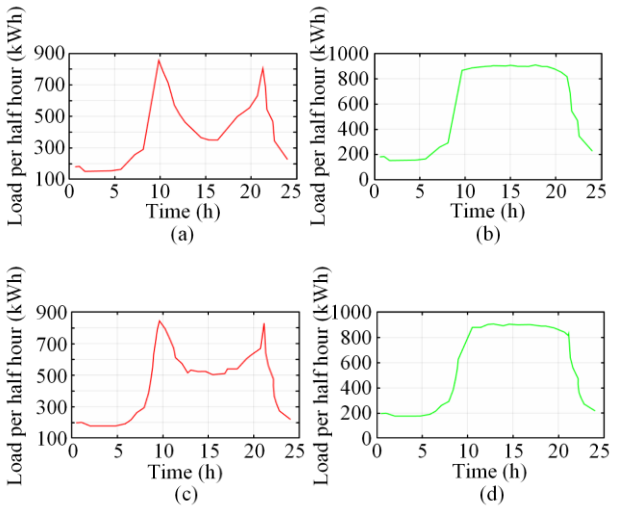

Fig. 14. Analyses of loads for different degrees of FCVs and EV. (a) Basic load for 80% FCVs + 20% EV. (b) Load with V2G for 80% FCVs + 20% EV. (c) Basic load for 20% FCVs + 80% EV. (d) Load with V2G for 20% FCVs+80% EV.

Figure 15 displays the analysis of basic load and loads with EV on different days. There are different numbers of vehicles visited and they are based on different charging demands. The charging demand in Monday is lower compared to Sunday.

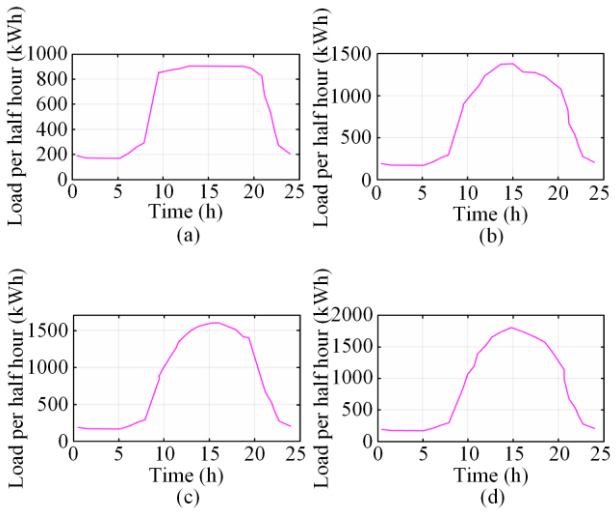

Fig. 15. Analysis of basic load and loads with EV on different days. (a) Basic load. (b) load with EV on day 1. (c) load with EV on day 6. (d) load with EV on day 7.

Figure 16 shows the analyses of various loads for Sunday. The increase in net income comes from less discharge loss of FCVs and less CO_2 emission, and income from offering vehicle to grid services.

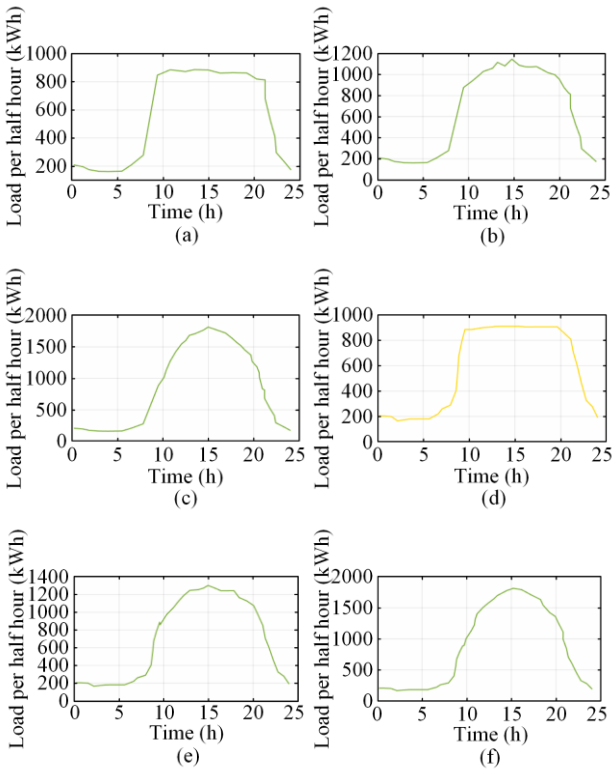

Fig. 16. Analyses of various loads for Sunday. (a) Basic load for Sunday, 100% FCVs. (b) Load with EV charging for Sunday, 100% FCVs. (c) Load with V2G for Sunday, 100% FCVs. (d) Basic load for 100% EV. (e) Load with electric vehicle charging for 100% EV. (f) Load with V2G for 100% EV.

Figure 17 displays the analyses of various loads for Monday. In 100% EV, the optimization curve ensures the maximal peak shaving. Because of higher income in FCVs, more power is released, and peak load is lower.

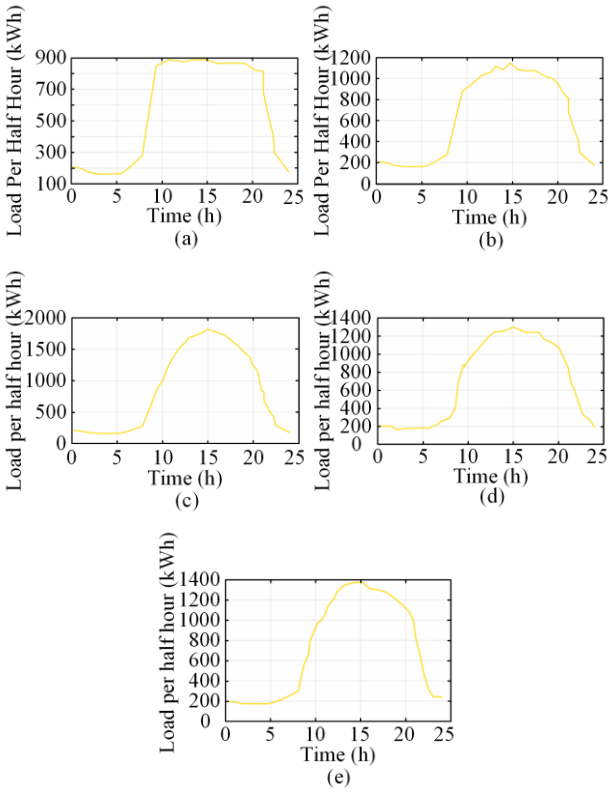

Fig. 17. Analysis of various loads for Monday. (a) Basic load for Monday 20% FCVs + 80% EV. (b) Load with EV charging for Monday 20% FCVs + 80% EV. (c) Load with V2G for Monday 20% FCVs + 80% EV. (d) Load with EV charging for 100% EV. (e) Load with V2G for 100% EV.

Figure 18 shows the analyses of various loads for Sunday. The effects of FCVs importation are slightly improved when the net income lessens with decrease in electricity price. When the price becomes 12.62 kWh, the total effectiveness of electric vehicle rapidly decreases. The direction of optimization changes from putting possible vehicles into V2G service to take peak cutting.

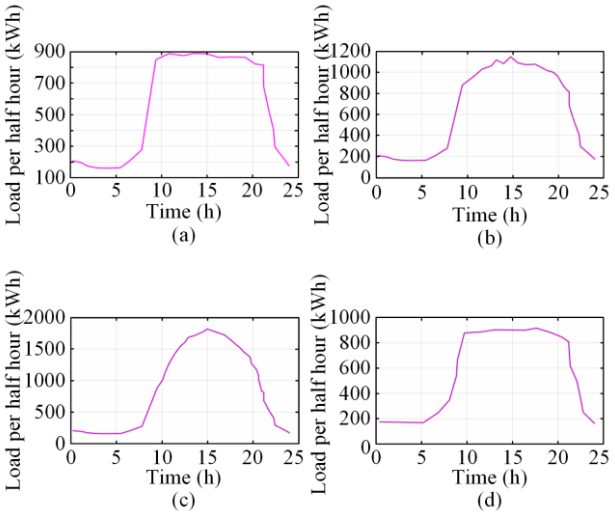

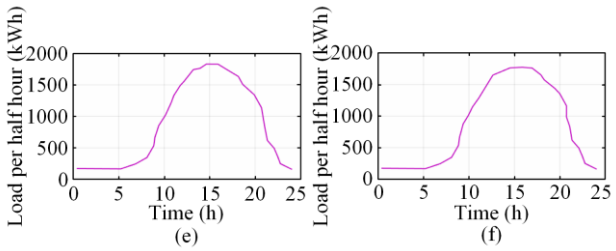

Fig. 18. Analysis of various loads for Sunday. (a) Basic load for Sunday 100% FCVs. (b) Load with EV charging for Sunday 100% FCVs. (c) Load with V2G for Sunday 100% FCVs. (d) Basic load for 100% EV. (e) Load with EV charging for 100% EV. (f) Load with V2G for 100% EV.

Figure 19 shows the analyses of various loads for Monday. The FCVs are steadier than EV while dealing with decrease in daily electricity price.

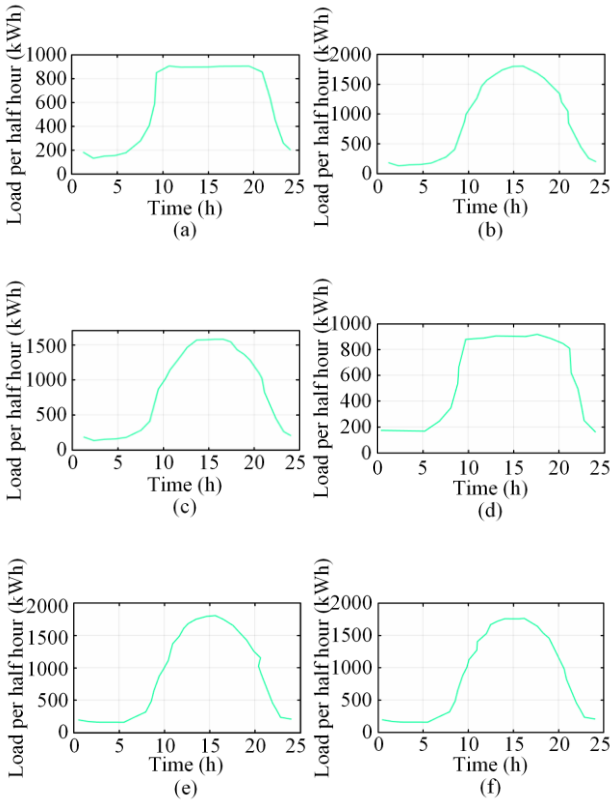

Fig. 19. Analyses of various loads for Monday. (a) Basic load for Monday 20% FCVs + 80%EV. (b) Load with EV charging for Monday 20% FCVs + 80%EV. (c) Load with V2G for Monday 20% FCVs + 80% EV. (d) Basic load for 100% EV. (e) Load with electric vehicle charging for 100% EV. (f) Load with V2G for 100% EV.

A. Sensitivity Analysis

Figures 20–22 show the total cost of Monday, Sunday and Saturday with EV charging demand, respectively.

Table II shows the sensitivity analysis of the proposed work, while Table III shows the results on Saturday, Sunday and Monday with EV charging demand.

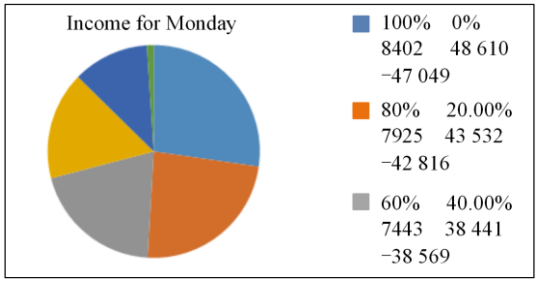

Fig. 20. Total cost of Monday with EV charging demand.

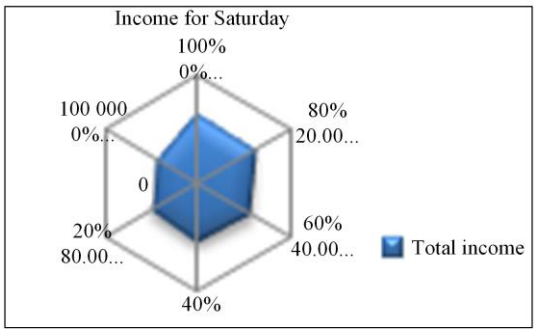

Fig. 21. Total cost of Sunday with EV charging demand.

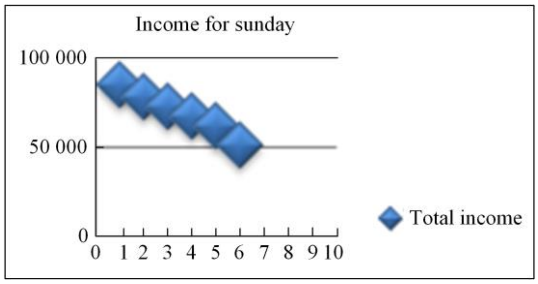

Fig. 22. Total cost of Saturday with EV charging demand.

TABLE II
SENSITIVITY ANALYSIS OF PROPOSED WORK

Variable	Description	Sensitivity
Initial investment	cost	High
Operating cost		Medium
Electricity demand	Building	High
Number of vehicle	FCEV	Medium
Fuel cell efficiency		High
Battery capacity	Energy storage	low
Renewable energy availability	RES	High
Grid electricity price	Price of electricity	Low

TABLE III
RESULT ON SATURDAY, SUNDAY AND MONDAY WITH ELECTRIC VEHICLE CHARGING DEMAND [18]

Monday (Price FCVs=29.21Yen/kW, Price EV= 24.02Yen/kWh)						
Proportion of EV	0%	20.0%	40.0%	60.0%	80.0%	100.0%
Proportion of FCVs	100%	80%	60%	40%	20%	0%
Peak cutting income	8402	7925	7443	6959	6692	732
V2G income	48 610	43 532	38 441	33 318	13 622	398
Total spending	−47 049	−42 816	−38 569	−34 290	−16 076	−749
Total income	9963	8640	7315	5987	4242	381
Saturday (Price FCVs=32.91Yen/kW, Price EV = 26.31Yen/kWh)						
Proportion of EV	0%	20.0%	40.0%	60.0%	80.0%	100.0%
Proportion of FCVs	100%	80%	60%	40%	20%	0%
Peak cutting income	22 686	21 860	21 755	20 746	19 721	18 703
V2G income	134 152	121 551	111 385	98 335	85 202	72 072
Total spending	−91 226	−81 999	−75 661	−65 966	−56 176	−46 419
Total income	65 611	61 412	57 479	53 115	48 746	44 355
Sunday (Price FCVs=33.15Yen/kW, Price EV = 26.51Yen/kWh)						
Proportion of EV	0%	20.0%	40.0%	60.0%	80.0%	100.0%
Proportion of FCVs	100%	80%	60%	40%	20%	0%
Peak cutting income	29 649	28 278	27 113	26 073	25 086	24 499
V2G income	176 437	159 215	142 280	125 546	109 044	80 364
Total spending	−12 1158	−10 8691	−96 047	−83 688	−71 673	−53 876
Total income	84 928	78 801	73 345	67 930	62 457	50 987

V. CONCLUSION

This paper assesses the economic advantages of FCV2G and FCVs marketing strategies. First, FCV2G potential is assessed, and the proposed controller is executed in MATLAB software and the performances of existing methods are also studied. Then, the performances of the proposed method and existing methods are plotted graphically. The proposed system easily coordinates energy flow between buildings and grid. When load usage is less than FCVs, excess electricity is sent to grid. The dynamic load profile is a function, and its performance is achieved in daily terms. The introduction of FCVs efficiently reduces the power demand of a target shopping mall based on real situation. The influences of FCV2G are investigated by comparing with EV, while MSA relates and examines the electricity price of discharge and the income of FCVs and EV is considered in 3 days: Monday, Saturday and Sunday. As FCVs imports grow, overall revenue increases. When importing 100%, overall revenue is 51.0% more than 100% EV, whereas peak-cutting and V2G service revenue are 30.5% and 95.0% greater, respectively. Low discharge loss, high capacity, and high discharge power are the main advantages of FCVs. FCV2G can improve FCVs and V2G promotions. The benchmark

FCVs ratio of 15% is used for sensitivity analysis. Results indicate that FCV2G benefits will improve with time. When the price of electricity increases on a daily basis, and the optimization direction attracts possible vehicles to engage in V2G service, the outcome shows that V2G income overtakes the total income. When the price of power increases and decreases on a daily basis, the benefits of peak-cutting overtake the total income and the optimization direction can be one of important economical approaches for lessening the peak loads.

ACKNOWLEDGMENT

Not applicable.

AUTHORS' CONTRIBUTIONS

Padhmanabhaiyappan Sivalingam: conceptualization, methodology, original draft preparation. Madhusudanan Gurusamy: supervision. Both authors read and approved the final manuscript.

FUNDING

This work is carried out without the support of any funding agency.

AVAILABILITY OF DATA AND MATERIALS

Not applicable.

DECLARATIONS

Competing interests: The authors declare that they have no known competing financial interests or personal relationships that could have appeared to influence the work reported in this article.

AUTHORS' INFORMATION

Padhmanabhaiyappan Sivalingam received the B.E. degree in Electrical and Electronics Engineering from Sengunthur Engineering College, Tiruchengode, India, in the year 2005 and the M.E degree in Power Electronics and Drives from Government College of Engineering, Salem, India, in the year 2007. He received his Ph.D. degree in Electrical Engineering from Anna University, Chennai in the year 2023. He is currently working as assistant professor at the SRM Valliammai Engineering College, Tamil Nadu, India. His research interests include the control of power converters, renewable energy and soft computing techniques. He published several technical papers in the national and international journal and conference. He is a member of the ISTE, IACST and IAENG. And his ORCID ID is: orcid.org/0000-0002-8894-0296.

Madhusudanan Gurusamy received the B.E. degree in Electrical and Electronics Engineering from Bharathidasan University, Trichy, Tamil Nadu, India, in 1997. He received the M.E. degree in Power Electronics and Drives from Bharathidasan University, Trichy, Tamil Nadu, India, in 2000, and the Ph.D. degree in Electrical Engineering from the National Institute of Technology, Tiruchirappalli, India, in 2020. From the year 2000 onwards, he has been working with the Department of Electrical Engineering SRM Valliammai Engineering College, affiliated to Anna University, Chennai, India. He is a member of IE(I), IEEE, ISTE and ISC. His research interests include renewable energy systems, energy storage system and power electronic controllers.

REFERENCES

[1] C. B. Robledo, M. J. Poorte, and H. H. M. Mathijssen *et al*., "Fuel cell electric vehicle-to-grid feasibility: a technical analysis of aggregated units offering frequency reserves," *Intelligent Integrated Energy Systems: the PowerWeb Program at TU Delft*, pp.167-194, Jan. 2019.

[2] T. U. Solanke, V. K. Ramachandaramurthy, and J. Y. Yong *et al*., "A review of strategic charging-discharging control of grid-connected electric vehicles," *Journal of Energy Storage*, vol. 28, no.1, Jan. 2020.

[3] P. Jain, A. Das, and T. Jain, "Aggregated electric vehicle resource modelling for regulation services commitment in power grid," *Sustainable cities and society*, vol.45, pp. 439-450, Feb. 2019.

[4] A. Alsharif, C. W. Tan, and R. Ayop *et al*., "A comprehensive review of energy management strategy in vehicle-to-grid technology integrated with renewable energy sources," *Sustainable Energy Technologies and Assessments*, vol.47, Jul. 2021.

[5] S. Goel, R. Sharma, and A. K. Rathore, "A review on barrier and challenges of electric vehicle in India and vehicle to grid optimisation," *Transportation engineering*, vol. 4, Feb. 2021.

[6] E. A. Moore, J. D. Russell, and C. W. Babbitt *et al*., "Spatial modeling of a second-use strategy for electric vehicle batteries to improve disaster resilience and circular economy," *Resources, Conservation and Recycling*, vol. 160, May 2020.

[7] V. D. W. M. Oldenbroek, V. Hamoen, and S. Alva *et al*., "Fuel cell electric vehicle-to-grid: experimental feasibility and operational performance as balancing power plant," *Fuel Cells*, vol. 18, no.5, pp. 649-662, Jul. 2018.

[8] B. Bibak and H. Tekiner-Moğulkoç, "A comprehensive analysis of vehicle to grid (V2G) systems and scholarly literature on the application of such systems," *Renewable Energy Focus*, vol.36, Nov. 2020.

[9] M. A. Hannan, M. S. Mollik, and A. Q. Al-Shetwi *et al*., "Vehicle to grid connected technologies and charging strategies: operation, control, issues and recommendations," *Journal of Cleaner Production*, vol. 339, Mar. 2022.

[10] Z. A. Arfeen, A. B. Khairuddin, and A. Munir *et al*., "En route of electric vehicles with the vehicle to grid technique in distribution networks: status and technological review," *Energy Storage*, vol. 2, no.2, Nov. 2019.

[11] A. Sangswang and M. Konghirun, "Optimal strategies in home energy management system integrating solar

power, energy storage, and vehicle-to-grid for grid support and energy efficiency," *IEEE Transactions on Industry Applications*, vol. 56, no.5, pp. 5716-5728, Sept. 2020.

[12] J. Liu, C. Zhuge, and J. H. C. G. Tang *et al*., "A spatial agent-based joint model of electric vehicle and vehicle-to-grid adoption: a case of Beijing," *Applied Energy*, vol. 310, Jan. 2022.

[13] Y. Li and S. Kimura, "Economic competitiveness and environmental implications of hydrogen energy and fuel cell electric vehicles in ASEAN countries: the current and future scenarios," *Energy Policy*, vol. 148, Jan. 2021.

[14] A. Benitez, C. Wulf, and A. de Palmenaer *et al*., "Ecological assessment of fuel cell electric vehicles with special focus on type IV carbon fiber hydrogen tank," *Journal of Cleaner Production*, vol. 278, Jan. 2021.

[15] C. Zhang, J. B. Greenblatt, and M. Wei *et al*., "Flexible grid-based electrolysis hydrogen production for fuel cell vehicles reduces costs and greenhouse gas emissions," *Applied Energy*, vol. 278, Nov. 2020.

[16] H. Li, B. Sun, and J. Hao *et al*., "Economical planning of fuel cell vehicle-to-grid integrated green buildings with a new hybrid optimization algorithm," *International Journal of Hydrogen Energy*, vol. 47, no. 13, pp. 8514-8531, Feb. 2022.

[17] F. Qian, W. Gao, and Y. Yang *et al*., "Economic optimization and potential analysis of fuel cell vehicle-to-grid (FCV2G) system with large-scale buildings," *Energy Conversion and Management*, vol. 205, Feb. 2020.

[18] M. İnci, M. Büyük, and M. M. Savrun *et al*., "Design and analysis of fuel cell vehicle-to-grid (FCV2G) system with high voltage conversion interface for sustainable energy production," *Sustainable Cities and Society*, vol. 67, Feb. 2021.

[19] A. Badji, D. O. Abdeslam, and D. Chabane, "Real-time implementation of improved power frequency approach based energy management of fuel cell electric vehicle considering storage limitations," *Energy*, vol. 249, Mar. 2022.

[20] A. Aljanad, A. Mohamed, and H. Shareef *et al*., "A novel method for optimal placement of vehicle-to-grid charging stations in distribution power system using a quantum binary lightning search algorithm," *Sustainable Cities and Society*, vol. 38, pp. 174-183, Apr. 2018.

[21] P. Thounthong, S. Pierfederici, and J. P. Martin *et al*., "Modeling and control of fuel cell/supercapacitor hybrid source based on differential flatness control," *IEEE Transactions on Vehicular Technology*, vol. *59,no.* 6, pp. 2700-2710, Jul. 2010.

[22] M. A. Al-Saffar and E. H. Ismail, " A high voltage ratio and low stress DC-DC converter with reduced input current ripple for fuel cell source," *Renewable Energy*, vol. 82, pp. 35-43, Oct. 2015.

[23] E. H. Ismail, M. A. Al-Saffar, and A. J. Sabzali, "High conversion ratio DC-DC converters with reduced switch stress," *IEEE Transactions on Circuits and Systems I: Regular Papers*, vol. 55, no. 7, pp. 2139-2151, 2008.

[24] L. Chuan and A. Ukil, "Modeling and validation of electrical load profiling in residential buildings in Singapore," *IEEE Transactions on Power Systems*, vol. 30, no. 5, pp.2800-2809, Feb. 2008.

[25] M. İnci, M. Büyük, and M.M. Savrun *et al*., "Design and analysis of fuel cell vehicle-to-grid (FCV2G) system with high voltage conversion interface for sustainable energy production," *Sustainable Cities and Society*, vol. 67, Feb. 2021.

[26] M. Sudha, M.R. Kandasamy, and M.S.S. Kumar, "A novel approach on cognitive radio sensor networks for efficient data transmission," *Wireless Personal Communications*, Jun. 2022.

[27] M. Dehghani and H. Samet, "Momentum search algorithm: a new meta-heuristic optimization algorithm inspired by momentum conservation law," *SN Applied Sciences*, vol. 2, no. 10, Sept. 2020.

[28] M. Inci, "Technoeconomic analysis of fuel cell vehicle-to-grid (FCV2G) system supported by photovoltaic Energy," *Energy Technology*, vol. 11, no. 4, Jan. 2023.

[29] C. Scott, M. Ahsan, and A. Albarbar, "Machine learning based vehicle to grid strategy for improving the energy performance of public buildings," *Sustainability*, vol. 13, no. 7, Apr. 2021.

[30] X. Pan, L. Wang, and Q. Qiu *et al*., "Many-objective optimization for large-scale EVs charging and discharging schedules considering travel convenience," *Applied Intelligence*, vol. 52, no. 3, pp. 2599-2620, Jun. 2021.

[31] X. Wei, K. W. Chan, and T. Wu *et al*., "Wasserstein distance-based expansion planning for integrated energy system considering hydrogen fuel cell vehicles," *Energy*, vol. 272, Mar. 2023.